

SOLID ROCKET MOTOR CERTIFICATION TO MEET SPACE SHUTTLE REQUIREMENTS:  
FROM CHALLENGE TO ACHIEVEMENT

John Q. Miller, National Aeronautics and Space Administration  
George C. Marshall Space Flight Center, AL and  
Joe C. Kilminster, Morton Thiokol, Inc., Brigham City, UT

ABSTRACT

The Solid Rocket Motor (SRM) for the Space Shuttle was by contract requirement, a state-of-the art motor design to the maximum extent possible.

There were three design requirements for which there was no existing solid rocket motor experience. These were: the requirement for a unique thrust-time trace to meet unique Space Shuttle requirements, the requirement for 20 uses of the principal hardware, and the requirement for a moveable nozzle with an 8° omniaxial vectoring capability.

These three unique requirements are discussed and the solutions presented.

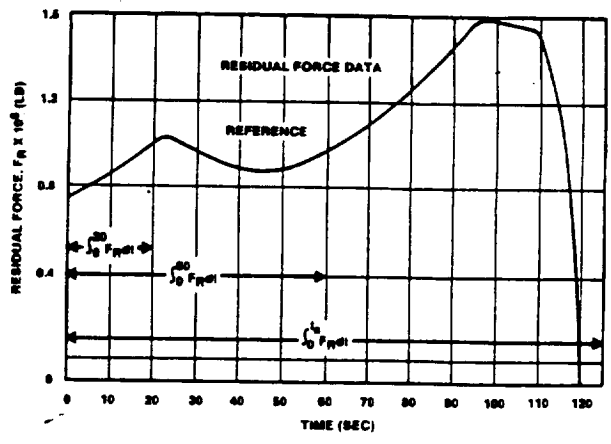
DESCRIPTION

THRUST-TIME TRACE

The development of the solid rocket motor thrust-time trace requirements and certification will be discussed.

Requirement

Establishment of the SRM thrust-time characteristic was based upon a residual force requirement derived from Shuttle system flight synthesis (Figure 1). Residual force is the force required to accelerate the Shuttle vehicle along a flight path after subtracting the thrust of the SSME's. Associated with this requirement was a vehicle liftoff thrust to weight ratio of 1.5, a maximum vehicle dynamic pressure of 650 psf, and a vehicle maximum acceleration limit of 3g. The specification of SRM residual force requirements enabled the SRM contractor to conduct design trade studies which culminated in the definition of a thrust-time history meeting system requirements. The results of these studies led to a more conventional definition of SRM thrust-time history requirements (Figure 2) which are currently included in the SRM Contract End Item specification.



Analytical Design Approach

The large size of the SRM, combined with a limited number of development tests (4), precluded a "cut-and-try" approach to curve shape tailoring. Rather, analytical assessments of the various mechanisms that can affect curve shape had to be made. Results of these assessments were then used as guidelines in establishing reasonable Contract End Item (CEI) specification limits on the nominal thrust trace shape. They also were used for contingency planning in the mandrel procurement, wherein enough flexibility was built into the initial mandrel configuration to counteract the most probable extremes in curve shape. The first two static tests (DM-1 and DM-2) showed that the actual curve shape, while containing some variations, was sufficiently close to the original prediction to preclude major mandrel modification.

NOMENCLATURE:  
 $F_{R_i}$  - INSTANTANEOUS RESIDUAL FORCE, LBF  
 $t_0$  - MAXIMUM ALLOWABLE ACTION TIME, SEC

FIGURE 1. SRM PERFORMANCE REQUIREMENTS

It was determined that the payload performance of the system was quite sensitive to the SRM thrust trace shape. In order to achieve sufficient control of the trace shape, Rockwell International (RI) and NASA decided to delineate requirements on the nominal thrust-time shape and also impose impulse gate requirements at 20 seconds and 60 seconds through which the impulse-time performance must pass.

The basic predictability limits that apply to the thrust-time curve shape of a solid rocket motor were analyzed based on previous large motor history. Results of this analysis were used to generate the envelope requirements within which the nominal thrust must fit and the impulse gate requirements on nominal performance (Figure 2).

Historic data were examined to determine the nature of the significant factors which contribute to predictability of solid motor ballistic performance. Examination was limited to those factors that contribute to predictability of thrust-time curve shape and thus affect the mandrel design. Easily countered factors such as the propellant burn rate were not considered, since a minor tailoring of the propellant formulation can easily modify the burning rate in accordance with a change in target rate. These changes can be implemented at any time in the program.

One of the most widely recognized factors that is not entirely predictable and which affects curve shape is erosive burning. Examination of large motor data, particularly Titan seven-segment data, indicated that large motor erosive burning did not significantly affect ballistic performance. It was concluded that limiting the Shuttle port mass velocities to levels at or below those experienced by the Titan seven-segment motors would preclude or minimize erosive burning.

Early in this literature search, a peculiar factor affecting curve shape was recognized. In many motors, both large and small, the actual trace shapes were more "humped" than the theoretical traces. Generally, actual traces are initially lower than the theoretical, higher in the middle of burn, and lower again near the end of web time. This phenomenon was given the acronym BARF--Burning Anomaly Rate Factor.

BARF was found in almost all of the 156 in. motors. It was also found in all the Aerojet 260 in. motors and apparently in the Titan seven-segment motor to a small degree. However, BARF did not occur in the Titan III C/D (five-segment motor). It is also found in many smaller motors, a notable example being the 5 in. circular perforation motor (5 in. CP) used by Thiokol for burn rate evaluation. A similar phenomenon is found in the Super BATES motor.

Based upon the frequency of occurrence of BARF in large motors, it was decided that the BARF phenomenon was a distinct possibility in the Shuttle SRM and that planning for the mandrel fabrication should include the flexibility to counter it, should it occur.

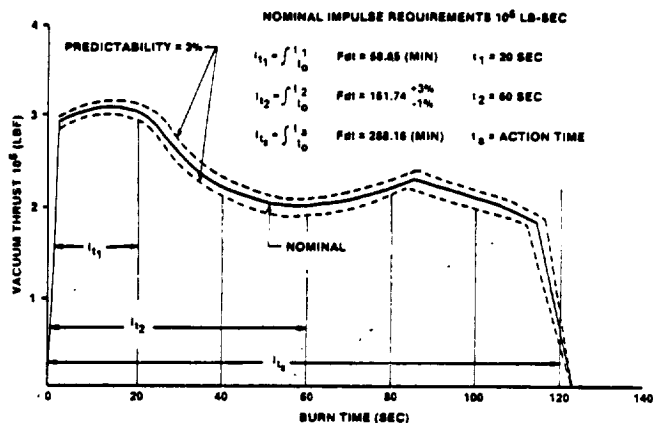
The other parameters which were considered potentially significant to a degree that could affect mandrel design were predictability of  $I_{sp}$  and nozzle throat erosion. It should be pointed out that the  $I_{sp}$  loss prediction technique was, at the time, in a relatively early stage of development. Since then, the model has been improved such that the prediction of delivered  $I_{sp}$  is well within 1%.

From the standpoint of mandrel design, a low  $I_{sp}$  is far more of a problem than a high  $I_{sp}$  because the constraint imposed by the maximum design pressure, used in the hardware design, precluded any increase in mass flow rate during the first 20 seconds without an increase in throat area. Any increase in throat area was precluded by hardware/schedule constraints. Thus the ability to recover from the effects of low  $I_{sp}$  impacts was considered in this analysis.

It should be noted that a 1% predictability degradation was being imposed upon a baseline nominal vacuum  $I_{sp}$  prediction of 262.2 seconds, which was itself felt to be slightly conservative since, at that time, the  $I_{sp}$  loss prediction technique indicated the  $I_{sp}$  would be slightly higher. The philosophy of introducing a small degree of conservatism into the prediction of  $I_{sp}$  was suggested by MSFC.

The nominal baseline vacuum specific impulse was conservatively predicted to be 262.2 seconds. The throat erosion rate was assumed to be 0.008 ips; and accuracy of throat erosion predictability was assumed to be  $\pm 15\%$ , based upon judgment of experienced nozzle designers.

It was assumed that  $I_{sp}$ , BARF and throat erosion rate were independent variables. This led to a statistical approach in the analysis wherein each effect was treated as an independent variable, and its effect was assessed independently. Impact of BARF on thrust performance is presented in Figure 3. The one percent low  $I_{sp}$  would result in a uniform one percent thrust reduction throughout operation.



NOTES: A)  $t_1$  - IGNITION TIME  
 B) THE NOMINAL THRUST-TIME CURVE OF THE QUALIFIED SRM MUST FALL WITHIN THE PREDICTABILITY ENVELOPE AND IS FURTHER CONSTRAINED BY THE TOTAL IMPULSE REQUIREMENTS

FIGURE 2. SRM NOMINAL PERFORMANCE REQUIREMENTS (VACUUM, 60°F)

Effect of throat erosion rate variation (+ 15%) proved to be minimal; at no time did the thrust deviation exceed 0.26% of nominal.

Since a mandrel modification after the first static test was allowed for in the planning, analytical grain design modifications were undertaken to counteract the effects of the assumed BARF and low  $I_{sp}$ .

Care was taken in the analytical redesign phase to limit the mandrel changes, since any mandrel modification is a relatively expensive, long lead time effort. Given this constraint, it was impossible to completely counteract these effects and small residual impulse deviations remained at the various gates as well as small residual deviations in the thrust-time curve shapes. The total residual thrust and impulse deviations at the various times were then determined by a root sum squaring of the three components. These residual deviations then formed the base for establishing specification limits, although more information was needed to completely quantify the limits.

Figure 4 presents the basic grain design. No design modifications were necessary to counteract low  $I_{sp}$  or to counteract BARF.

At this point, information was not available to completely quantify CEI specification limits on impulse gates and the thrust envelope. This was because the grain design modifications were to be made only after one motor firing and there was a distinct possibility that it would not be a nominal motor, due to normal ballistic performance reproducibility. Further, the accuracy of the data acquisition system (+ 0.5%) impact on these uncertainties needed to be assessed and added into the specified tolerances.

The potential dispersion that a particular motor could have from the nominal performance of a population was estimated by reviewing Stage I Minuteman data. A population of 23 motors was examined to determine the coefficient of variation in impulse yielded at 38% of web burn. This variation, when multiplied by an appropriate K factor, was assumed to represent the maximum limit that the DM-1 impulse could be dispersed from the true population nominal at 20 seconds (17.8% of web burn) and 60 seconds (53.3% of burn) with a 90% confidence and 99% probability. The resulting dispersion was 1.55%. This also is a reasonable estimate for the instantaneous thrust dispersion at any time.

The assessment of impulse reproducibility at a fixed percent web burn was made to factor out the effect of burn rate, since predictability of nominal burn rate was not a pertinent variable in this study.

The total potential dispersion in impulse values at 20 and 60 seconds and in the thrust time curve were then estimated by root-sum-squaring the residual components due to BARF,  $I_{sp}$  predictability, throat erosion rate predictability, normal motor reproducibility, and instrumentation accuracy. Tables I and II present the value of each component and the total (RSS) value, respectively, for impulse gates and thrust-time curve, and compare these estimates to those finally selected for the CEI specification.

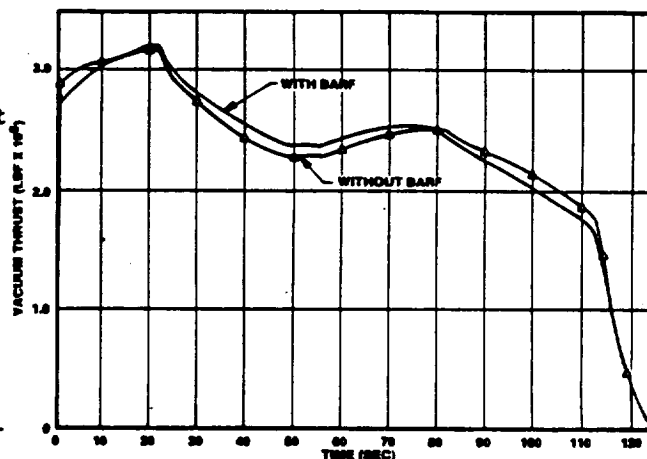


FIGURE 3. EFFECT OF BARF ON TC-227A-75 THRUST PERFORMANCE

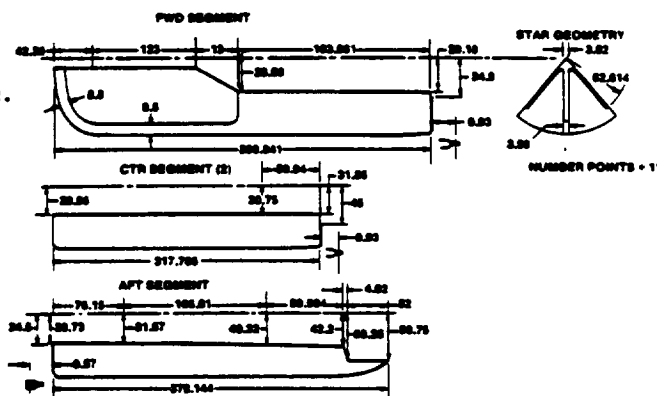


FIGURE 4. BASIC GRAIN DESIGN

TABLE I  
POTENTIAL DEVIATION FROM PREDICTED IMPULSE AT 20 SEC, 60 SEC, AND ACTION TIME

Time (sec)	Nominal Predicted Vacuum Impulse (Nlb-sec)	Potential Deviation From Predicted Normal (%)					Total (RSS)	Selected CEI Specification Limit About Population Nominal (%)
		Due to BARF	Due to $I_{sp}$	Due to Throat Erosion	Due to Instrumentation	Due to Motor Reproducibility		
20	60.03	0.611	1.017	0.06	0.90	1.525	+ 2.0	-2.0 (minimum)
60	161.74	0.178	0.479	0.125	0.90	1.525	+ 1.7	+3.0, -1.0
Action Time	291.07	0.070	0.872	0.130	0.90	0.0	+ 1.0	-1.0 (minimum)

TABLE II  
POTENTIAL DEVIATION FROM PREDICTED THRUST AT VARIOUS TIME

Time (sec)	Nominal Predicted Vacuum Thrust (lb)	Potential Deviation From Predicted Nominal Thrust, Percent Nominal					Total (RSS)	Selected CEI Specification Limit About Population Nominal, % Nominal
		Due to BARF	Due to Low $I_{sp}$	Due to Throat Erosion	Due to Instrumentation	Due to Motor Reproducibility		
1	2,849,000	+0.663	-0.718	0.0	± 0.5	± 1.5	1.9	3.0
10	3,065,000	+1.095	-0.852	0.05	± 0.5	± 1.5	2.1	3.0
20	3,157,000	-0.394	-1.017	0.10	± 0.5	± 1.5	1.9	3.0
30	2,729,000	+0.465	+4.504	0.13	± 0.5	± 1.5	4.8	3.0
40	2,453,000	-0.487	+5.992	0.17	± 0.5	± 1.5	6.2	3.0
50	2,259,000	-0.436	+1.195	0.21	± 0.5	± 1.5	2.0	3.0
60	2,325,000	-0.233	-1.831	0.25	± 0.5	± 1.5	2.4	3.0
70	2,465,000	-0.321	-1.962	0.25	± 0.5	± 1.5	2.7	3.0
80	2,523,000	-0.542	-2.324	0.25	± 0.5	± 1.5	2.9	3.0
90	2,330,000	-1.428	-2.588	0.26	± 0.5	± 1.5	3.4	3.0
100	2,131,000	+1.243	-2.862	0.26	± 0.5	± 1.5	3.5	3.0
110	1,881,000	+1.228	-2.355	0.26	± 0.5	± 1.5	3.1	-3.6 +3.0
120	416,000	-3.299	-6.331	0.26	± 0.5	± 1.5	7.3	-87.6 +54.6

### Test Results

Data from the first two static test firings were analyzed and, based upon these data, the following observations were drawn.

1. No erosive burning was observed.
2. The BARF phenomenon did not occur.
3. Vacuum delivered specific impulse was about 265 seconds, based upon expended propellant weight.

4. During the first 6 seconds, flow conditions in the star region produced head-to-aft end stagnation pressure drops in excess of theoretical one-dimensional predictions. The flow field in the star region appears to offer the most reasonable explanation for this phenomenon. The flow in the valleys at the aft end of the star, where the valleys end (Figure 4), must be directed radially inward towards a central core of axial flow. At the star/CP transition, this core must be constrained to the diameter of the CP. If throughout the star the flow is contained within approximately this diameter, the effective port area for axial flow is considerably less than the star cross-sectional port area. The resulting pressure drops, due to axial velocity, would be of the magnitude observed. This effective port area then gradually increases until around 6 seconds, when the full port area of the star is utilized for axial flow and measured pressure drops are in good agreement with theoretical predictions.

Since there was such excellent agreement between the predicted curve shape made with the analytical model and test data, no major mandrel modification from the DM-1 configuration was required to satisfy nominal curve shape and impulse gate requirements. Figure 5 compares the projected final flight motor configuration thrust-time performance with the CEI thrust requirements, and Table III compares the projected 20 and 60 second impulse values with specification requirements. As can be seen, the nominal thrust performance will essentially satisfy the requirements in all areas.

## SOLID ROCKET MOTOR CASE

The overall design philosophy for the Solid Rocket Motor case was to develop a simple, rugged and effective design based upon the use of proven techniques and concepts. Major emphasis was placed on reusability and performance reproducibility.

Each motor case consists of 11 individual case segments that are assembled into casting segments prior to propellant loading. The casting segments consist of two interchangeable center segments and forward and aft segments. There are four deliverable casting segments per SRM.

The intent here is to discuss those criteria, testing and certification requirements affecting the reusability of the SRM case.

### Design Requirements

The design requirements for the Space Shuttle SRM case were evolved from three major sources: those specified by the contracting organization (NASA), those self-imposed by the motor manufacturer (Thiokol) and those which inherently exist due to fabrication, processing and transportation limits. It is not within the scope of this paper to list all requirements, but rather to list only the requirements which were considered to be the major drivers in the evolution of the current case design.

#### Basic Strength/Toughness/Elongation

Minimum ultimate tensile strength = 195 ksi  
 Minimum tensile yield strength = 180 ksi  
 Typical fracture toughness = 90 ksi $\sqrt{\text{in}}$ .  
 Minimum elongation = 8%  
 Minimum reduction in area = 25%

#### General Safety Factors

Before SRM separation  
 Yield factor of safety = 1.10  
 Ultimate factor of safety = 1.40

After SRM separation  
 Yield factor of safety = 1.10\*  
 Ultimate factor of safety = 1.25\*

#### Safety Factors for Pressures

Before SRB separation  
 Yield pressure = 1.2 x limit pressure  
 Ultimate pressure = 1.40 x limit pressure

After SRB separation (water recovery, etc.)  
 Yield pressure = 1.10\* x limit pressure  
 Ultimate pressure = 1.25\* x limit pressure

\* This is a design goal only for water impact loads.

The SRM case and its components must be capable of reuse following recovery and retrieval after submersion in sea water for up to seven days (168 hrs.) The SRM case and its components must meet the refurbishment and reuse cycle that supports the Space Shuttle System turnaround time from lift-off to lift-off.

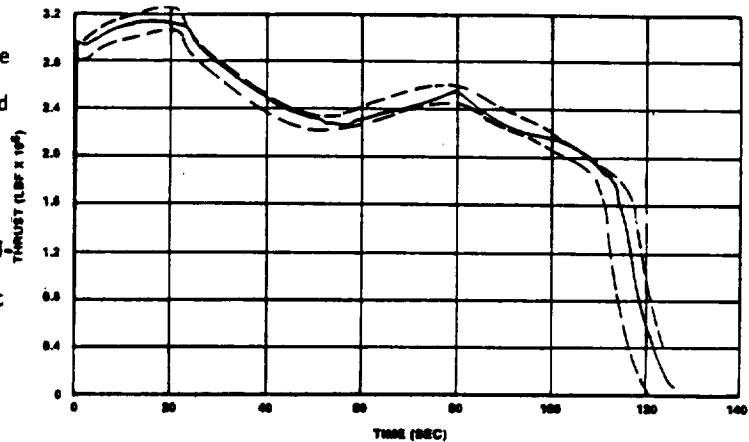


FIGURE 5. SRM-3 PRELIMINARY PREDICTION

TABLE III

FLIGHT MOTOR SRM IMPULSE COMPARED WITH  
 CEI REQUIREMENTS NOMINAL, 60°F

Time (sec)	CEI Required Impulse (Mlb-sec)		Predicted Impulse (Mlb-sec)
	Min	Max	
20	58.83	----	61.20
60	160.12	166.69	164.89
Action Time	288.16	----	293.63



TABLE IV  
SUMMARY OF JOINT TESTS

Specimen	Test No.	Type	Test	Failure Load (10 <sup>6</sup> lb)	Factor of Safety	Cycles	Remarks
1	1	5 Pin - Nominal	Burst	1.04	2.23	---	Pin and clevis arm failure.
2	2	5 Pin - Nominal	Burst	1.00	2.27	---	Pin and clevis arm failure.
3	3	5 Pin - Nominal	Cyclic and Burst	1.01	2.17	240	After cycling, no pin marked and minor hole elongation. Clevis arm failure.
4	6	5 Pin - Oversize Hole (0.010 in. large dia)	Burst	1.00	2.15	---	Clevis holes bearing failure. Clevis arms spread.
5	5	4 Pin - Nominal	Burst	0.80	2.15	---	Specimen did not separate. Pin bending and clevis hole bearing failure.
6	7	5 Pin - Bushing (0.050 in. wall thickness - DGAC)	Cyclic and Burst	1.025	2.20	160	No bushing deformation after cycling. Clevis arm failure.
7	4	5 Pin - 1st Flaw (0.050 deep - Jewelers File)	Cyclic and Burst	0.80	1.72	160	No crack growth. Notch failure between tang holes at 800 K.
8	8	5 Pin - 2nd Flaw (0.050 deep - EPDM)	Cyclic and Burst	0.855	1.83	160	Crack between tang holes at 685 K on burst cycle. Burst 855 K.
9	9	5 Pin - Low K <sub>IC</sub> - Flaw (0.050 deep - EPDM)	Cyclic and Burst	0.825	1.77	1	Crack between holes at 453 K during 1st cycle at tang flaw.
10	10	5 Pin - Corrosion	Cyclic and Burst	1.025	2.20	240	Clevis Failure.

4 Pin Joint  
Limit Load = 373,000 lb (Maximum Flight Load)  
Ultimate = 1.4 Limit = 523,000 lb

5 Pin Joint  
Limit Load = 466,000 lb (Maximum Flight Load)  
18 $\frac{1}{2}$  Proof = 515,000 lb  
Ultimate = 1.40 Limit = 653,000 lb

The first requirement stipulates that the largest flaw which can escape detection with specified NDI will not grow to critical size through 20 uses of the case. One use of the case encompasses all events associated with its use as it proceeds through the fabrication, loading, launch, recovery, refurbishment and proof test sequence. Compliance to this requirement is demonstrated through the application of principles of linear fracture mechanics.

The second requirement for the SRM case associated with fracture mechanics/flaw growth principles requires that the case be proof tested prior to flight to a load level which will screen out (by case failure) all existing flaws which are critical for flight, or would become critical if the flaw were allowed to grow (theoretically) through four missions. One mission is defined as one motor operating (pressure) cycle plus one water impact sequence.

#### MOVABLE NOZZLE WITH 8<sup>0</sup> OMNIAXIAL VECTOR CAPABILITY

The Solid Rocket Motor nozzle is a convergent-divergent moveable design containing an aft pivot point flexible bearing as the gimbal mechanism (Figures 8 and 9). The nozzle is partially submerged to minimize erosive conditions in the aft end of the motor and to fit within envelope length limitations. The nozzle provides attach points for the thrust vector control (TVC) actuators, an attachment structure to mate with the motor aft closure, a capability for jettisoning a part of the aft exit cone after burnout to reduce water impact damage to the nozzle flexible bearing.

TVC for the Space Shuttle SRM is obtained by omniaxis vectoring of the nozzle. The vector requirements of the system, the impact of multiple reuse on the components, and the unique problems associated with a large flexible bearing are discussed. The subscale bearing development program is also presented.

#### Requirements

Omniaxial requirements for the SRM nozzles are shown in Figure 10. The 7.1 deg of nozzle vectoring required in the vehicle's pitch and yaw axes decreases to 5 deg in the 45 deg plane between the pitch and yaw axes. By locating the actuators in this 45 deg plane, they could be designed with a stroke equivalent to 5 deg, yet, when operated in unison, provide the total 7.1 deg required in the

pitch and yaw planes. The flexible bearing which permits the movement of the nozzle was designed for a maximum omniaxial nozzle vectoring of  $\pm 8$  deg; thus, allowance of 0.9 deg was incorporated in the design to allow for geometric misalignment and actuator overtravel. Requirements for the nozzle bearing are tabulated on Table V.

The requirement was placed upon the nozzle flexible bearing elastomer that it be reused nine times. The reuse requirement was a significant driver in the design of the nozzle flexible bearing. Components were designed so that they would withstand the high loads encountered at the time of water impact.

#### Flexible Bearing Design

The flexible bearing consists of alternate lamina of natural rubber elastomer and steel shims between a forward and aft end ring (Figure 11). Ten metal shims and 11 layers of elastomer are vulcanized to each other and the end rings. The elastomer provides the flexibility that permits the nozzle to vector. The flexible bearing is designed to be used 10 times without replacing the elastomer pads. After each flight the flexible bearing is disassembled from the nozzle and placed in a test fixture, where extensive tests are conducted to insure its integrity prior to reuse in another nozzle. Calculations and subscale test data show that the elastomer will be suitable for a minimum of 10 uses. Should the testing between flights indicate that the bearing elastomer has been damaged during a flight or recovery operation, the bearing can be disassembled by cutting it apart and the metal parts can be refurbished and reused. The parts can then be cleaned and the bearing remolded with new elastomer pads. Experience in the flight program has shown that bearing reuse is feasible and a bearing in STS-7 has been used three times in static tests as well as on STS-2 flight.

#### Testing

The flexible bearing is the largest ever built for a flight program. While the design concepts were state-of-the-art, it was deemed advisable to conduct a development program to assure that the bearing could

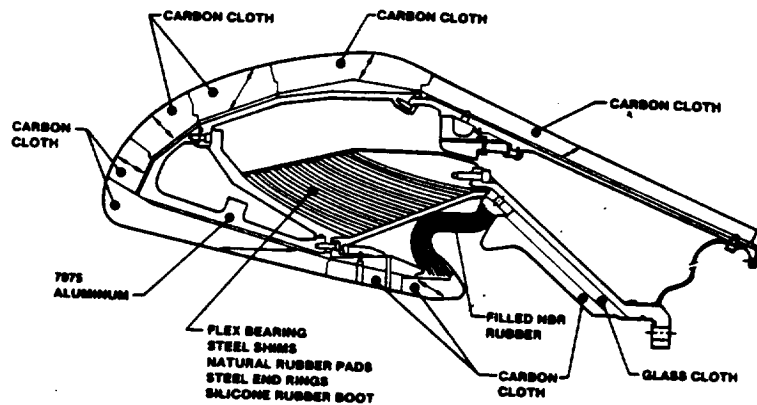


FIGURE 8. NOZZLE FORWARD ASSEMBLY

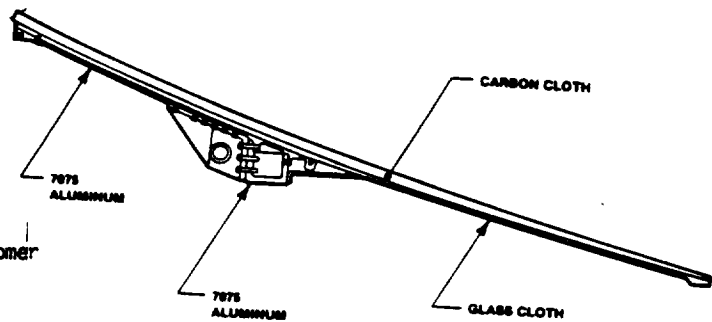


FIGURE 9. NOZZLE EXIT CONE ASSEMBLY

#### OMNIAXIAL DEFLECTION REQUIREMENT

- 7.1 DEG CONTROL REQUIREMENT
- 0.9 DEG GEOMETRICAL MISALIGNMENT
- 0.4 OVERTRAVEL
- 8.6 TOTAL OMNIAXIAL REQUIREMENT

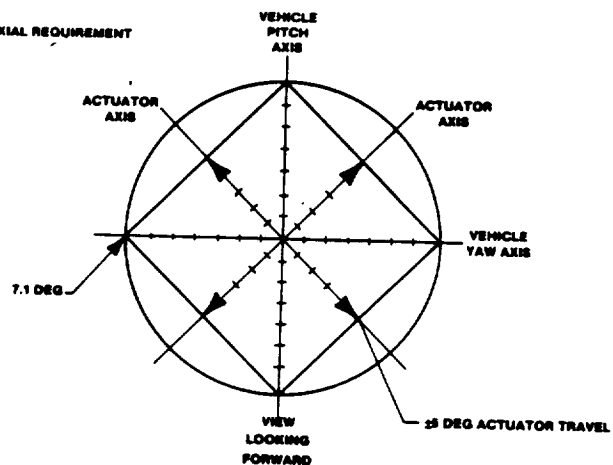


FIGURE 10. SOLID ROCKET MOTOR TYC REQUIREMENTS

be reused as required and to obtain performance characteristics such as torque, various spring constants, and the center of rotation when vectored. The development program consisted of fabricating three subscale bearings approximately one-quarter size (Figure 12) and three full size prototype bearings. Two of the three subscale bearings were, in fact, true geometric subscales designed by scaling all of the dimensions to approximately one-quarter the size of the full size bearing. The other subscale was of the same general size as the first two, but had only two metal shims and three elastomer pads, whose thicknesses were not scaled down but were the same as on the full scale bearing. The true subscale 10-shim bearings were fabricated and tested and provided data which, when scaled up to full size, indicated that the performance of the bearing would be acceptable. The bearings have also been vectored through duty cycles equivalent to the actual flight service (plus acceptance testing) that would be experienced in 10 flights. These data indicated that the fatigue characteristics of elastomer are adequate for the 10 uses required.

The major problems in the development of the full size flex bearing were the complexity of the mold (Figure 13) necessary to fabricate the bearing and the requirement to uniformly heat the rubber to the 300°F temperature without overheating the rubber next to the heating elements. Several of the early bearings experienced uneven heating and the subsequent lack of vulcanization between the rubber pads and metal shims. A very severe test has been developed where the flex bearing is longitudinally stretched two inches and inspected for unbonds. This test has shown that while several of the early bearings lacked areas of vulcanization and had to be disassembled and rebuilt, the more recent bearings have all been properly vulcanized.

The two-shim subscale bearing was primarily designed to provide processing data to confirm that thick pads of elastomer could be manufactured that would have the desired fatigue characteristics. Some performance data were also obtained with this bearing.

As mentioned, three prototype flexible bearings were also included in the development program. These bearings were fabricated and extensively tested to confirm that performance was within specifications and that the fatigue life of the elastomer in the flexible bearing environment meets the minimum 10-use criteria. These three bearings also provided repeatability data and confirmed that the abbreviated acceptance tests to be conducted on each bearing prior to use are adequate to insure that it is suitable for reuse.

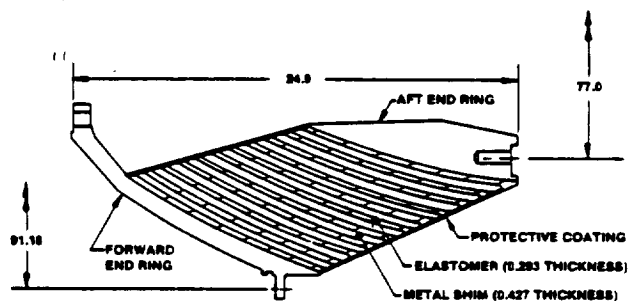
### CONCLUSIONS

There have been four development motor tests and three qualification motor tests in the basic SRM development program. There have been six DDT&E (twelve instrumented SRM's) flights.

All pressure-time traces for the development, qualification and flight test motors in the DDT&E program, (less STS-6, data not yet available) when corrected to standard burn rate, pressure and propellant mean bulk temperature have fallen well within the predictability limits established in the CEI specification (Figure 14).

TABLE V  
NOZZLE BEARING DESIGN REQUIREMENTS

Omniaxial Vector Capability	±8 deg	
Actuator Stall Load	103,424 lb	
Plane of Actuator		
Total Use Requirements		
Metal Parts	20 times	
Bearing Elastomer	10 times	
Safety Factors	Prior to Separation	After Separation
Structure	1.4 Ultimate	1.25 Ultimate
Nonpressure Vessel	1.1 Yield	1.1 Yield
Pressure Vessel	1.2 Yield	1.2 Yield



WEIGHT SUMMARY (LB)

FORWARD END RING	1.367
SHIMS	3.767
ELASTOMER	291
AFT END RING	1.532
MISCELLANEOUS	43
TOTAL	6,880

FIGURE 11. FLEXIBLE BEARING CROSS SECTION

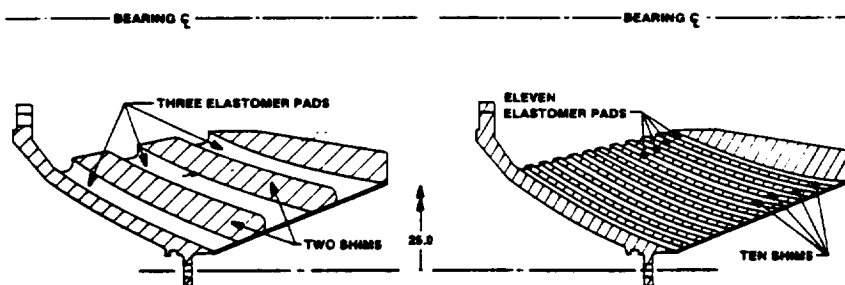


FIGURE 12. SUBSCALE FLEXIBLE BEARING DETAILS

42 motor case components used in static firings during the development program have been reused in flight. DDT&E flight six had 4 motor case components reused from DDT&E flight one.

A nozzle flexible bearing has been reused three times during the DDT&E program. Four nozzle flexible bearings have been reused in the DDT&E flight program, and one of the nozzle flexible bearings in STS-6 was reused from DDT&E flight one. It was nearly 5 years old. In all cases the demonstrated torque has been less than the limits established in the CEI specification.

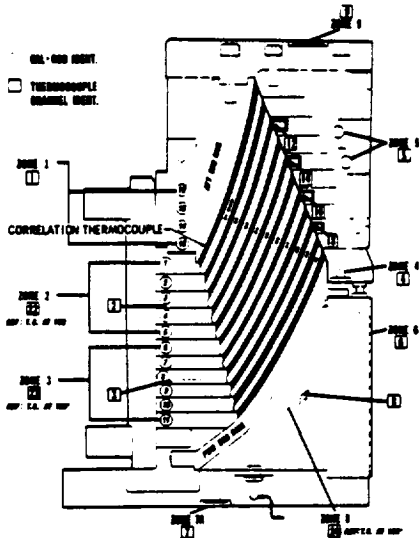


FIGURE 13. NOZZLE FLEXIBLE BEARING MOLD

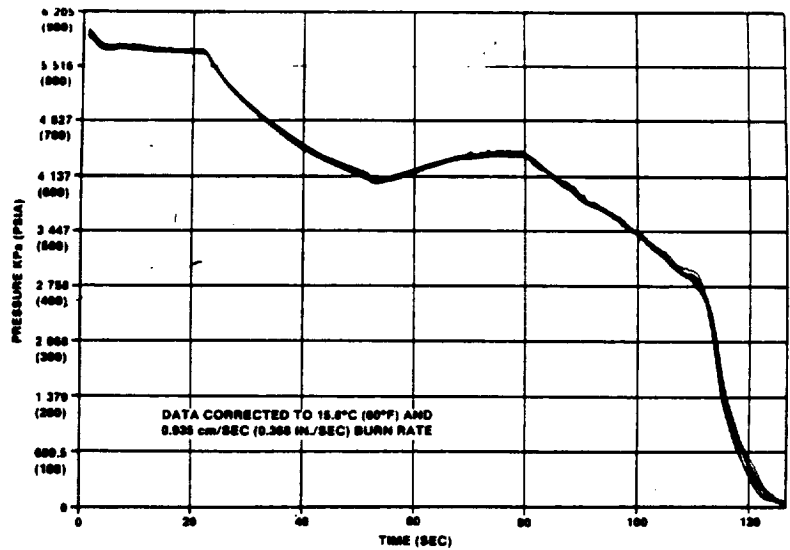


FIGURE 14. COMPOSITE OF 13 BASELINE SIM PRESSURE TRACES

ORIGINAL PAGE IS  
OF POOR QUALITY.